

Supplementary Information

for

Alumina-supported sub-nanometer Pt₁₀ clusters: amorphization and role of the support material in a highly active CO oxidation catalyst

Chunrong Yin, Fabio R. Negreiros, Giovanni Barcaro, Atsushi Beniya,
Luca Sementa, Eric C. Tyo, Stephan Bartling, Karl-Heinz Meiwes-Broer, Sönke Seifert,
Hirohito Hirata, Noritake Isomura, Sandeep Nigam, Chiranjib Majumder,
Yoshihide Watanabe, Alessandro Fortunelli, and Stefan Vajda

Table of Content

Materials and Methods

- Figure S1.** Arrhenius plot and the calculated activation energy.
- Figure S2.** Evolution of the XANES spectra of Pt₁₀ clusters under reaction conditions.
- Figure S3.** Typical topographic images, histograms of apparent cluster height and histograms of apparent cluster aspect ratio (=apparent height/apparent diameter) of Pt₁₀/Al₂O₃/NiAl(110).
- Figure S4.** Line profiles of apparent height of as deposited Pt₁₀ clusters and after CO and O₂ exposure at 27 °C.
- Figure S5.** STM images at room temperature (a) and 150 °C (b) after CO and O₂ gas exposure.
- Figure S6.** LEED images of Al₂O₃/NiAl(110) and Pt₁₀/Al₂O₃/NiAl(110).
- Figure S7.** XPS spectra of Pt₁₀ clusters on Al₂O₃/NiAl(110) after CO and O₂ gas exposure.
- Figure S8.** Low-lying isomers of free Pt₁₀, magnetic moments of the isomers, adsorption energies of O₂ or CO molecules adsorbed on selected configurations of free Pt₁₀, and spin density for the global minimum and a higher-energy isomer of free Pt₁₀.
- Figure S9.** Pictorial images of the structures of Pt₁₀ systems supported on alumina, to complement Fig. 4 of the main text: bare Pt₁₀, Pt₁₀ with O₂ or two O adatoms, Pt₁₀ with CO, Pt₁₀ systems with co-adsorbed O₂ and CO; first step of CO_{ox}, at low coverage on the pyramidal configuration and at high coverage.
- Figure S10.** Breaking of O₂ on Pt₁₀ starting from O₂ in the gas phase and then adsorbed on a bridge site. Each red cross represents one NEB image. The energy barrier for O-O bond breaking is ≈0.3 eV.
- Figure S11.** Plot of the energy as a function of time during a 4-psec Molecular Dynamics simulation at 300 K starting from a OOCO intermediate adsorbed on gas-phase Pt₁₀.
- Figure S12.** Results of local minimizations after adding one additional CO or O₂ molecule on the highlighted sites of the Pt₁₀(O₂)₂(CO)₃ cluster, showing desorption of CO or O₂ molecules initially positioned next to the cluster sites highlighted by circles (the species relax away into the gas phase) and thus proving that the cluster is locally saturated.
- Figure S13.** Bader charge analysis of two selected configurations Pt₁₀(O₂)₂(CO)₃ and Pt₁₀O₂(CO)₂(O)₂.

References

Materials and Methods

Experimental Section I – Clusters on alumina film prepared by atomic layer deposition (ALD)

Preparation of the amorphous ALD-alumina film. Amorphous alumina is chosen as support material because it resembles the catalyst carrier widely used in industry and it has been proven excellent at immobilizing nanometer and subnanometer sized clusters.¹⁻⁴ In the present study a 3 monolayer thick (~0.7 nm) film is prepared by atomic layer deposition (ALD) on top of the native oxide of a N-type (phosphorus doped) silicon wafer.

Cluster deposition I. The ALD-alumina supported Pt₁₀ catalyst is synthesized by soft-landing size-selected metal clusters from a molecular beam generated in a laser vaporizations source. The cluster deposition apparatus is described in detail elsewhere.^{2-3, 5-6} In brief, the molecular beam of platinum clusters is generated by laser evaporation of a rotating platinum rod using helium as carrier gas. Next, an assembly consisting of ion optics and quadrupole mass filter guide the positively charged Pt clusters into the deposition chamber to deposit positively charged clusters consisting 10-atom Pt clusters (with traces of about ~10% of 8- and 9- atom clusters) on the alumina support. The cluster deposition spot is about 3mm in diameter, and during deposition the silicon wafer is moved by a manipulator to accommodate three separate spots on the chip. The loading of deposited Pt is determined by online monitoring of the cluster flux on the support with a picoammeter. A coverage of 0.05 atomic monolayer (ML) equivalent of Pt (1 ML corresponds to 1.5×10^{15} Pt atoms/cm², the density of a Pt(111) surface.⁷) is applied on each spot to avoid possible aggregation upon landing of the clusters. After deposition, the sample is taken out of the chamber for further combined catalytic testing and *in situ* characterization by X-ray scattering, and X-ray absorption performed at Sector 12-ID-C at the Advanced Photon Source of the Argonne National Laboratory.

Catalytic testing. Temperature programmed reactions (TPRx) are conducted within a fixed-bed, continuous flow reactor.⁸ The certified gas mixtures (10% CO and 10% O₂, air gas) are configured into CO:O₂:He=1:1:98 with a total flow rate of 30 sccm by using calibrated mass flow controllers (Brooks model SLA5850 and 0154). The pressure inside the reactor is kept constant at 800 Torr by automated computer control. The sample is placed on the top of the ceramic heater (Momentive Performance Materials Inc.) with a K-type thermocouple attached to the side of the heater. A temperature profile depicted in [Figure 1a](#) is programmed with a temperature controller (Lakeshore model 340) and a deviation less than 0.5 °C is achieved. The sample is heated with a slow heating rate of 10°C/min up to 300°C with a step of 50°C and is kept at each temperature step for 30 mins. To minimize the background and to get flat baseline for all interested masses, considerable care is taken during purging of the reactor, and then a continuous flow of helium and reactants cleans the reactor for another 4.5 hours before TPRx started. After TPRx, the gas is changed to 10% oxygen to monitor possible changes in the oxidation state of Pt upon the removal of the CO from the feed. During TPRx the reactants and products are monitored using a differentially pumped mass spectrometer (Pfeiffer Vacuum Prisma Plus QMS 220). The spectrometer is operated in multi-ion-detection mode (MID) and

intensity at mass to charge ratios of 28, 32 and 44 is recorded for CO, O₂ and CO₂ respectively. To quantify the reaction turn-over rate (TOR), the sensitivity of the mass spectrometer is calibrated by using certified gases with known concentration of the monitored reactant and product species. The TOR data reported here are background corrected which means that the CO₂ signal detected over the blank alumina thin film (i.e. without Pt clusters present) is subtracted from the CO₂ signal collected over the Pt₁₀ sample. After background correction, the CO₂ signal is converted into TOR based on the known Pt metal loading. The estimated uncertainty in the determined TOR value is around 5% or better.

Synchrotron in situ characterization. In-situ GIXANES and GISAXS are performed with the same reactor during TPR_x studies. The GIXANES detected in fluorescence mode was set at Pt L₃ edge to examine the evolution of oxidation state of Pt during CO oxidation. GIXANES data are collected using a four-element Vortex detector mounted perpendicular to the beam. The photon energy is scanned between 11.25 and 12.05 keV. The collected data are analyzed with IFEFFIT interactive software package (with ATHENA and ARTEMIS graphical interfaces).⁹ The GIXANES spectra for a wide range of bulk Pt standards are collected to perform energy calibration and quantification of oxidization state of the Pt catalysts. Since PtO is thermally unstable, we select Pt foil, (NH₄)₂PtCl₄ and PtO₂ as Pt(0), Pt(II) and Pt(IV) standards a linear combination fitting was performed and the results summarized in [Figure 1b](#). The linear combination fitting using bulk standards provides a general trend as the function of environment and reaction temperature for the evolution of the composition (i.e. oxidation state) of the clusters. GISAXS with a geometry optimized for particles above 1nm is used to monitor possible sintering during heat treatment under catalytic conditions. The GISAXS data are collected on a platinum detector (1024×1024 pixels) with X-rays of 11.5 keV as a function of temperature. The two-dimensional GISAXS images are then cut both in horizontal and vertical directions. The scattering from the cluster sample is then compared with the background scattering of a blank support.

Experimental Section II. – Clusters on alumina film grown on NiAl(110).

Growth of the crystalline alumina film. The preparation of the alumina film is performed in ultrahigh vacuum chambers connected with each other ($<1 \times 10^{-8}$ Pa). The clean NiAl(110) surface is prepared by several cycles of Ar-ion sputtering, followed by annealing at 1300 K. The thin alumina film is prepared by dosing 1800 L (Langmuir: 1×10^{-6} Torr s) oxygen at 600 K followed by annealing at 1100 K for 5 min. The process is repeated to eliminate and close open metal patches in the film.

Cluster deposition II. Pt-cluster ions are produced by a dc magnetron sputtering cluster source. Size-selected Pt₁₀ cluster ions are deposited on Al₂O₃/NiAl(110) from the surface normal at 300 K. The kinetic-energy distribution of Pt₁₀⁺ clusters is measured by a retarding potential method using a metal plate at the sample position. Full width at half maximum of the energy distribution is 11 eV. The impact energy is tuned to 0.67 eV/atom by adjusting a bias voltage of 48 V applied

to the surface (soft-landing condition). The total amount of Pt deposited, determined from the integrated Pt_{10}^+ neutralization current on the sample, is 7.5×10^{12} atoms/cm² in a deposition area with diameter ~ 10 mm.

STM Characterization. STM measurements are performed at room temperature using a low-temperature STM (LT-STM, Omicron GmbH) with a Nanonis controller (SPECS Zurich GmbH) and a tungsten tip.

Treatment under reaction conditions. We perform the high-pressure gas treatment under 800 Torr with CO and O₂ seeded in He. The concentration of CO as well as O₂ was 1% (i.e. partial pressures of 8 Torr). These conditions are identical to those to which the Pt₁₀/ALD-alumina system is subjected. The high-pressure gas treatment is performed using the high-pressure reaction cell, which constitutes a micro batch reactor in the 800 Torr pressure range under practical conditions.¹⁰

Theoretical Section – Computational approach

Gas phase systems. For the DFT calculations on Pt₁₀ clusters in the gas phase, the Quantum Espresso¹¹ plane-wave self-consistent field code (PWscf) is used, employing the Perdew-Burke-Ernzerhof (PBE)¹² exchange-correlation functional and ultra-soft pseudopotentials.¹³ The following parameters are selected in the geometry optimizations within the global optimization search using the basin-hopping algorithm (see below): wave-function and charge-density cutoffs equal to 15 and 90 Ry, respectively, a face centered Bravais cubic cell with side length equal to 19 Å, a Gaussian smearing of 0.02 Ry, and a convergence threshold for self-consistency equal to 10⁻⁶ Ry. Geometry optimizations are performed spin restricted and using only the Gamma-point for the integration in the reciprocal space. In a second step, the lowest-energy structures found by the global search using the previous numerical parameters are re-optimized with a higher accuracy: wave-function/charge-density cutoffs of 40/320 Ry, respectively, smearing of 0.005 Ry, and spin unrestricted.

Alumina-supported systems. For the DFT calculations on Pt₁₀ clusters supported on an alumina surface, calculations are also performed using the plane-wave pseudo-potential method as implemented in the Vienna *ab initio* Simulation Package (VASP)¹⁴, with the electron-ion interaction described by the full-potential all-electron projector augmented wave (PAW) method.¹⁵ As in the gas phase, spin polarized calculations are performed using PBE exchange-correlation functional.¹² The cut off energy for the plane wave basis set is 30 Ry. The geometries are considered to be converged when the forces on each atom become 0.01eV/Å or less. The total energy convergence is tested with respect to the plane-wave basis set size and simulation cell size, and the total energy is found to be accurate within 1 meV. The α -Al₂O₃(0001) surface is modeled with 18-atomic layer slab by truncating the bulk α -Al₂O₃ structure (a=b= 4.766 Å and c= 12.999 Å). It should be noted that in this model hydroxyl groups on the alumina surface are not considered. Experimentally, hydroxyls are found at ambient conditions, but their number gradually decreases as the temperature is raised until they finally disappear around ~ 500 °C.¹⁶

Our model thus represents an alumina which, being fully dehydroxylated, realizes maximum adhesion of Pt clusters. Together with the results in the gas phase, this allows us to bracket the system's energetics and catalytic behavior. To avoid interactions between periodic slabs, we use a vacuum of 13 Å between slabs. A large 3 x 3 supercell (30 atom/per unit cell) is used to avoid interactions between images. Overall super-cell dimensions are 14.30 x 14.30 x 25.99 Å containing 270 atoms. A Monkhorst–Pack set of 5 x 5 x 1 K-points is used throughout all the calculations. For structural relaxation, all 18 atomic layers are allowed to relax including a dipole correction¹⁷ to avoid any error due to interaction between adjacent images.

Structural search. The search for the most stable structures for the Pt₁₀ cluster in the gas phase is performed using a Basin-Hopping (BH) global search algorithm¹⁸ coupled with a DFT evaluation of energy and forces (i.e., a DF/BH algorithm).¹⁹⁻²⁰ We deploy a total of 400 BH Monte-Carlo steps, random moves of 1.4 Å in the Cartesian directions of each atom, and a fictitious temperature $k_B T$ in the Monte-Carlo acceptance criterion of 0.4 eV. Once the most stable Pt₁₀ structures are identified, the adsorption of one to few CO and/or O₂ molecules is investigated, considering each distinct adsorption site on the Pt₁₀ cluster and including the possibility of adsorbing more than one CO molecule on the same site. This search provides a picture of the energetics of CO/O₂ adsorption on 10-atom Pt clusters and – as a side-information – the number of CO/O₂ molecules needed to reach saturation. In addition, in the case of co-adsorption of CO and O₂, configurations corresponding to the formation of complexes containing CO₂/CO₃ species are also considered. In the end, for each composition: Pt₁₀(O₂), Pt₁₀(CO), Pt₁₀(CO)(O₂), etc., a total of 5-20 different configurations are optimized and analyzed. Transition states are determined using the nudged elastic band (NEB) algorithm²¹ using the Broyden scheme in a two-step approach: a first NEB on the full reaction path using 5-8 intermediate images and a somewhat lower accuracy (wave-function and charge density cutoffs in the range of 25/150 Ry to 35/280 Ry) in order to speed up this first path search, followed by a second NEB calculation with initial and final states close to the previously determined transition state, using 3 intermediate images and the climbing-image procedure to refine the value of the energy barrier and the transition state geometry. Structural search for supported clusters is much less exhaustive due to the cpu-demanding character of such simulations. Configurations selected from the most stable in the gas phase according to previous experience are positioned on the alumina surface, trying to explore as diverse an epitaxy as possible, and locally minimized. NEB calculations are performed with using 5-8 intermediate images as in the gas phase.

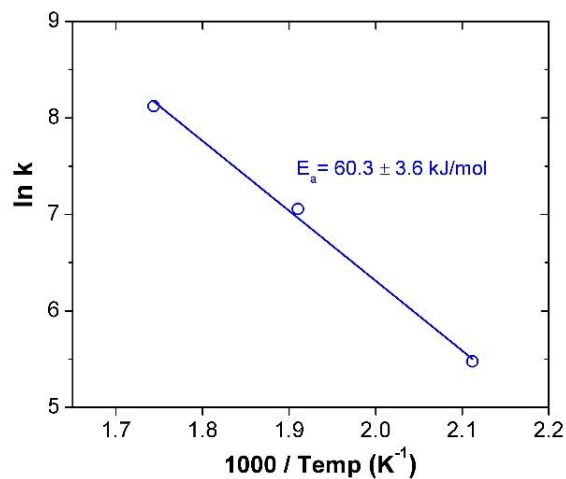


Figure S1. Arrhenius plot and the calculated activation energy.

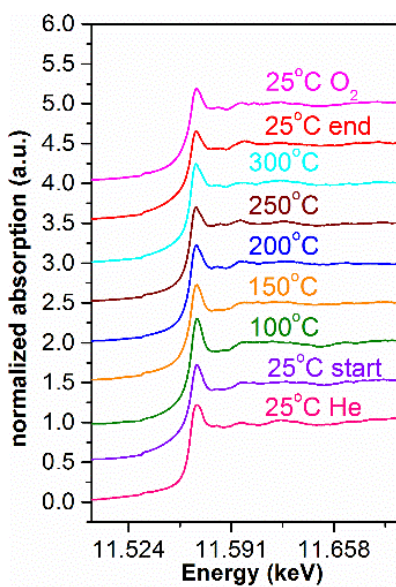


Figure S2. Evolution of the GIXANES spectra of Pt₁₀ clusters (from the bottom to the top): 1) 25 °C He: spectrum recorded at room temperature in helium prior the inlet of the reaction mixture, 2) spectra recorded during the heating ramp under the mixture of CO and O₂ in helium and 3) spectrum taken after cooling back to room temperature, under O₂ in helium.

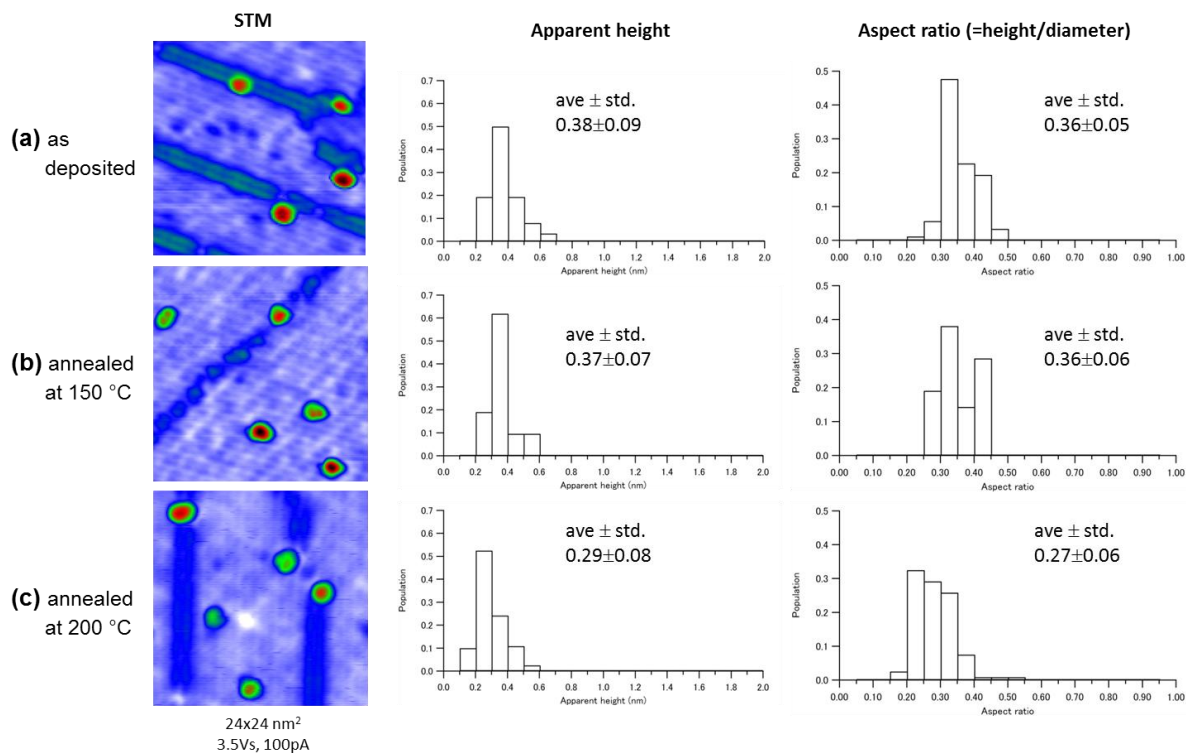


Figure S3. Typical topographic images, histograms of apparent cluster height and histograms of apparent cluster aspect ratio (=apparent height/apparent diameter) of Pt₁₀/Al₂O₃/NiAl(110) after 30 minute heat-treated at each temperature under vacuum, (a) as deposited, (b) 150 °C and (c) 200 °C, respectively. Note that the apparent aspect ratio can be estimated lower than the real value under the strongly influenced in diameter compared with height by the tip convolution effect.²²

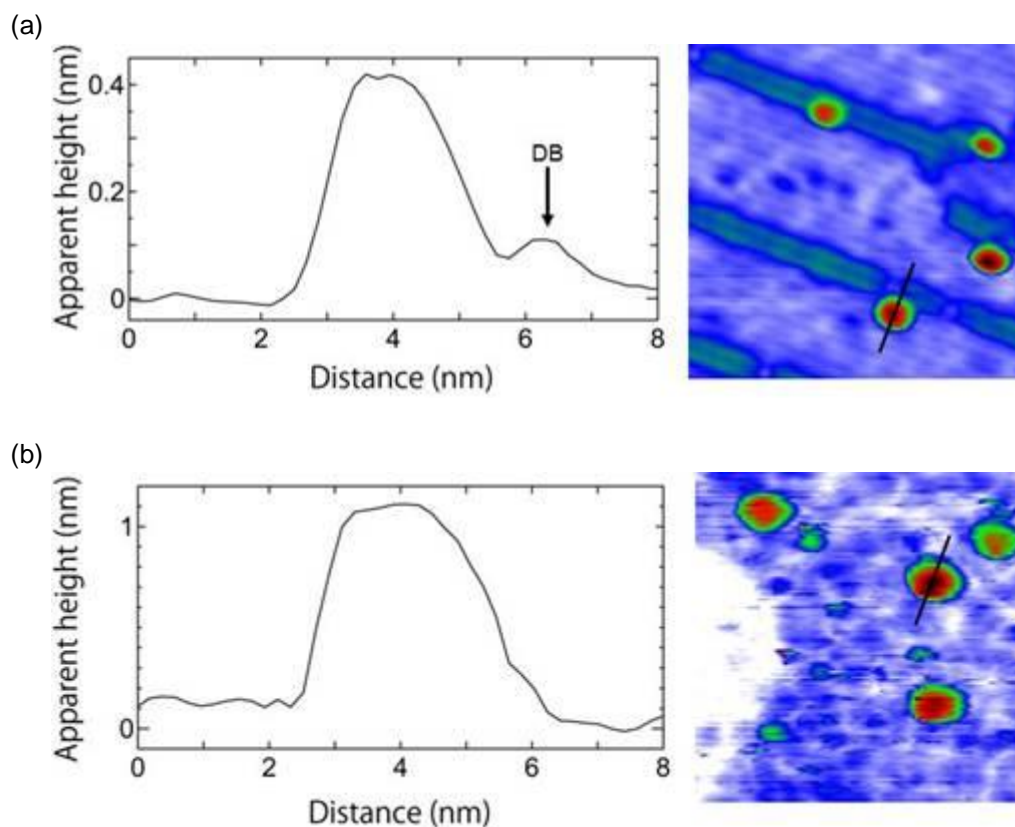


Figure S4. Line profiles along the black line in each STM image (3.5Vs, 100pA) of Pt₁₀ clusters on Al₂O₃/NiAl(110) (a) as deposited, (b) after CO and O₂ exposure at 27 °C. The resolved domain boundary is indicated by arrow in the plot. The change in the apparent height of the clusters shows the transition to a multilayered Pt structure. As described in the main text, the real cluster height of as deposited Pt clusters can be estimated²³⁻²⁴ as $\sim 0.38 + 0.33 - 0.5 = 0.21$ nm (i.e. single Pt layer, 2D structure), where 0.38 nm is the clusters' apparent height, 0.33 nm is the alumina film's apparent height, and 0.5 nm is the geometric height of the Al₂O₃ film estimated in [Figure S7\(c\)](#). Consequently, the real cluster height under CO and O₂ exposure can be estimated at least $1.1 + 0.33 - 0.75 = 0.68$ nm, corresponding to a 2 or 3 Pt-layer structure (i.e. 3D structure), where 1.1 nm is the clusters' apparent height, 0.33 nm is the alumina film's apparent height, and 0.75 nm is the geometric height of the Al₂O₃ film estimated in [Figure S7\(c\)](#).

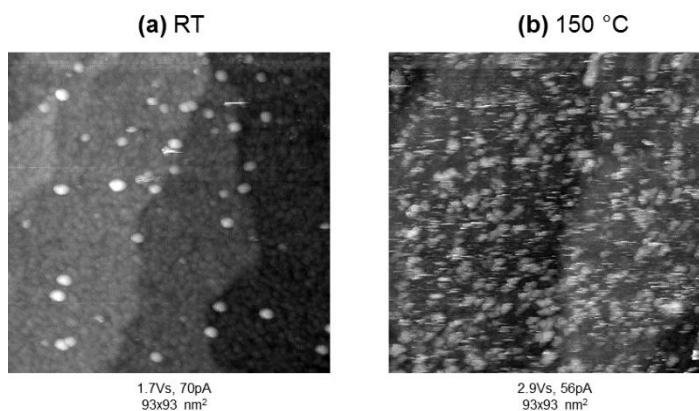


Figure S5. STM images of $\text{Pt}_{10}/\text{Al}_2\text{O}_3/\text{NiAl}(110)$ after CO and O_2 gas exposure (a) at room temperature and (b) $150\text{ }^\circ\text{C}$. Note that after exposure and elevated temperature the atomic steps were distinguishable, thus the atomic resolution was preserved during the experiment.

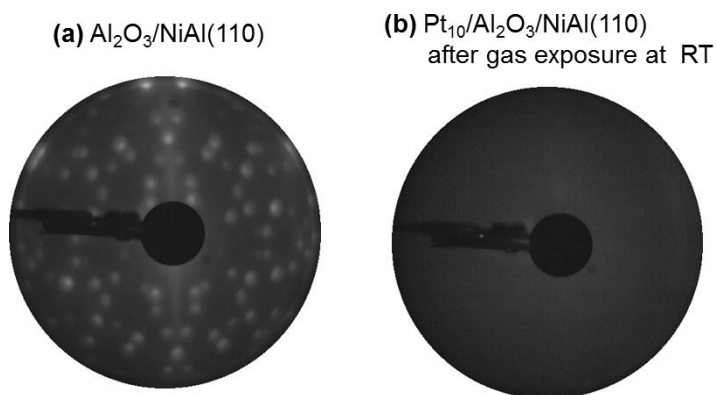
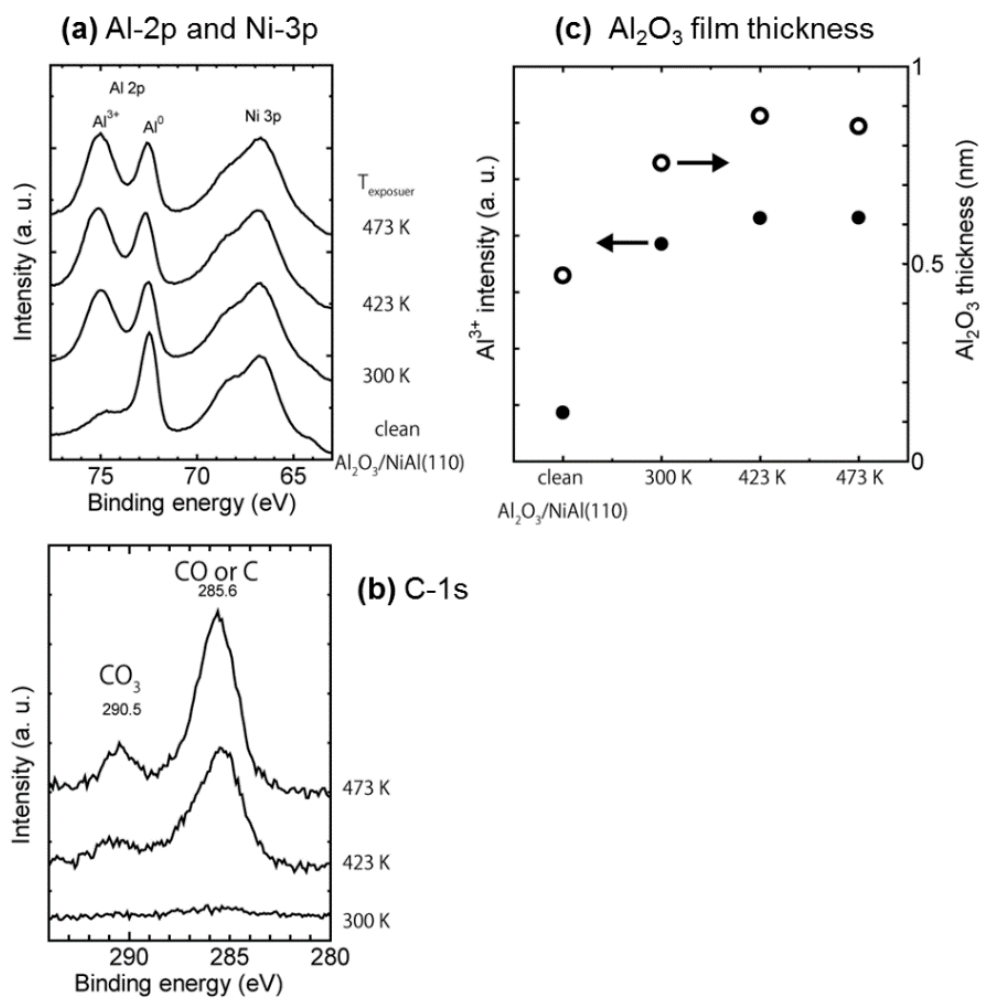


Figure S6. LEED images of (a) $\text{Al}_2\text{O}_3/\text{NiAl}(110)$ and (b) $\text{Pt}_{10}/\text{Al}_2\text{O}_3/\text{NiAl}(110)$ after gas exposure. The energy of the primary electrons was $E_0 = 50\text{ eV}$.



FigureS7. XPS spectra of $\text{Pt}_{10}/\text{Al}_2\text{O}_3/\text{NiAl}(110)$ after CO and O_2 gas exposure. (a) Al2p and Ni3p spectra, (b) C 1s spectra, (c) Al_2O_3 film thickness estimated from Al^{3+} intensities.²⁵

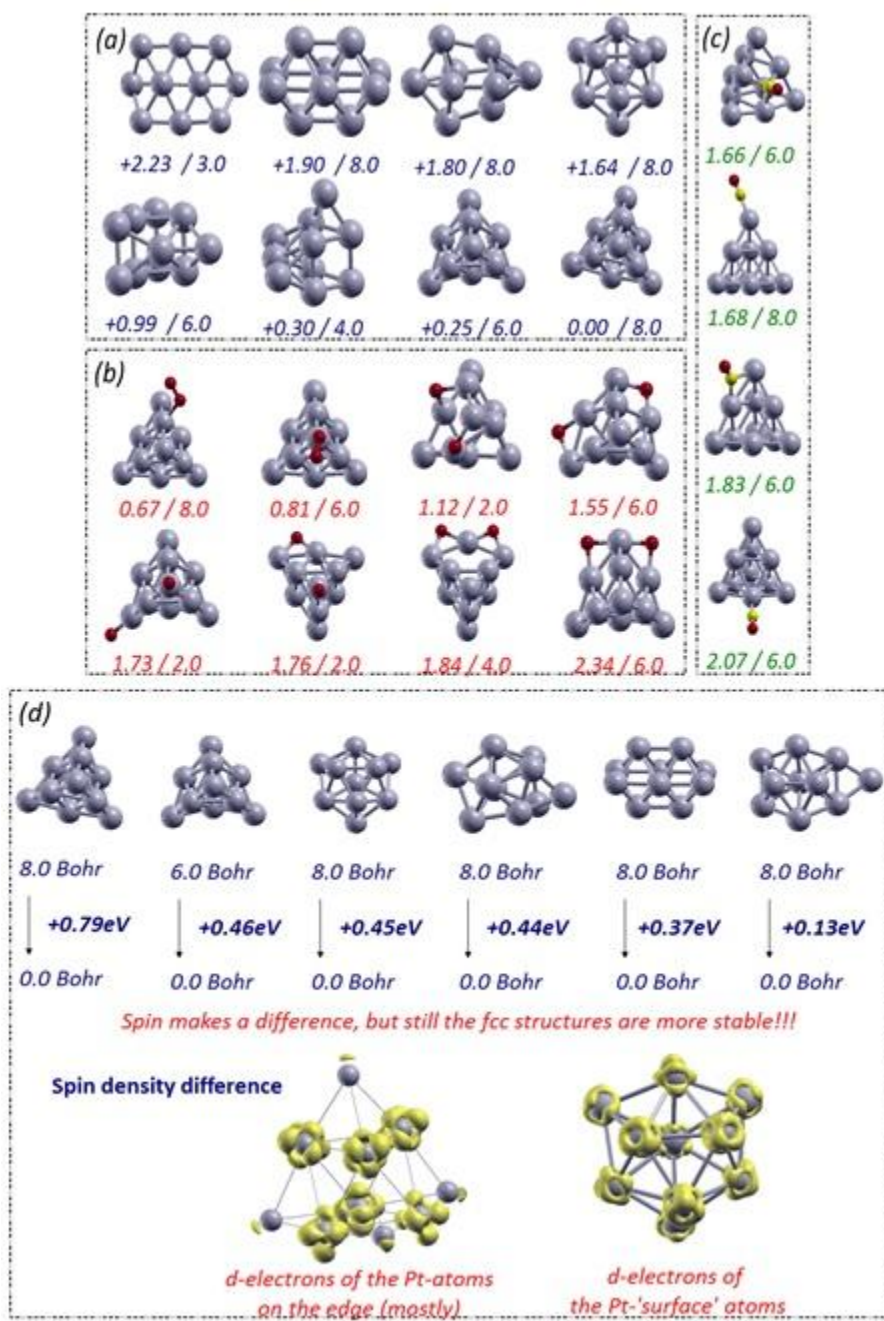


Figure S8. (a) Low-lying isomers of free Pt₁₀: energy differences with respect to the global minimum are reported in eV; next to this value, the magnetic moment (in Bohr magneton units) of each isomer is reported. The Pt₁₀ global minimum has a pyramidal shape, followed by a slightly rearranged pyramid (0.25 eV), a configuration of mixed decahedral-fcc character (0.3 eV), a bilayer arrangement (higher in energy by 1 eV), and other higher energy isomers including a planar structure above 2 eV. Adsorption energies (in eV) and spin moment of the total system (in Bohr magneton units) of (b) O₂ or (c) CO molecules adsorbed on selected configurations of free Pt₁₀. (d) Energy differences of selected isomers after quenching the magnetic moment. Plots of spin density for the global minimum and a higher-energy isomer of free Pt₁₀.

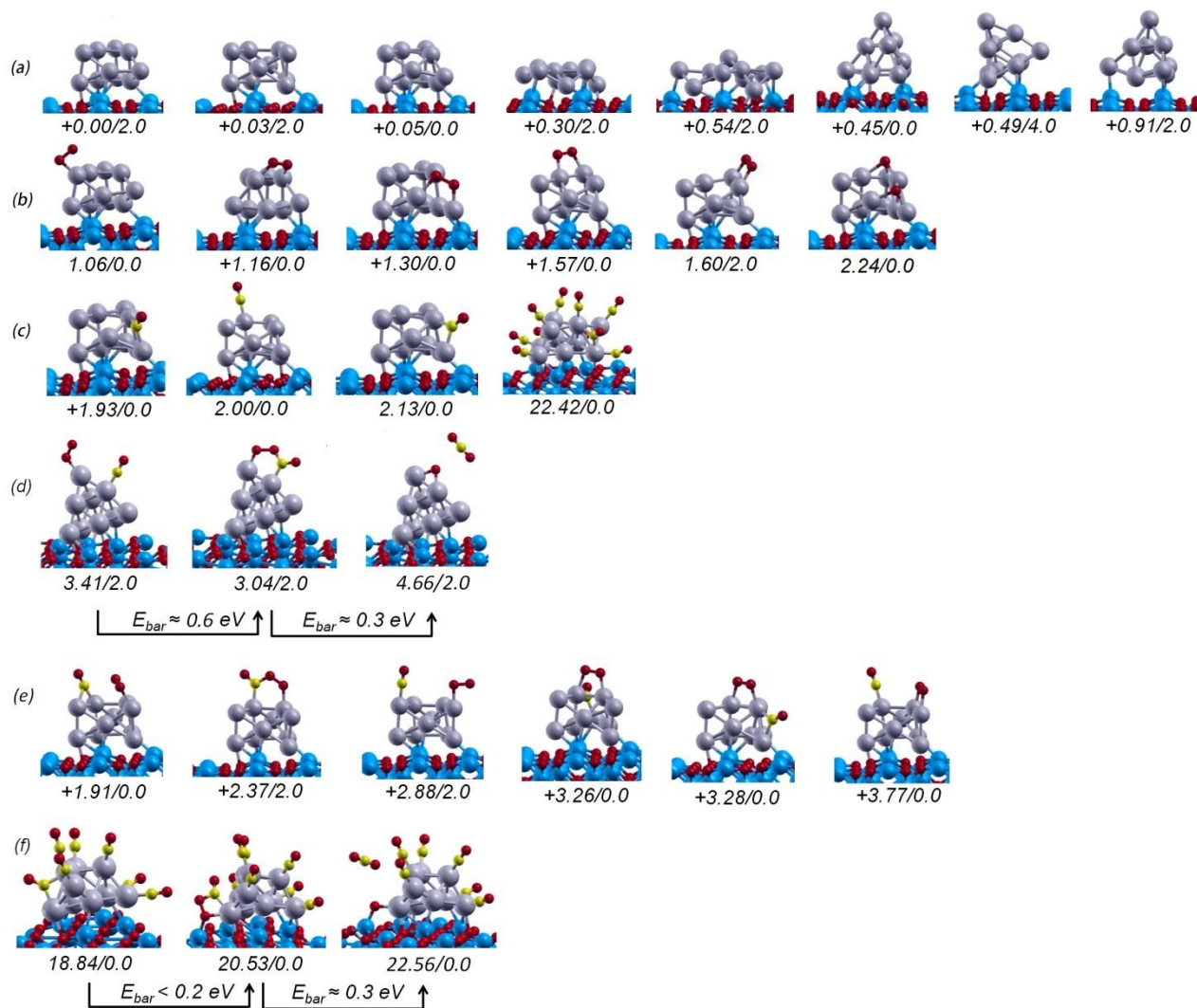


Figure S9. Pictorial images of the structures of Pt_{10} systems supported on alumina, to complement Fig. 4 of the main text: (a) bare Pt_{10} ; (b) Pt_{10} with O_2 or two O adatoms; (c) Pt_{10} with CO; (e) Pt_{10} systems with co-adsorbed O_2 and CO; (d,e) first step of COox (d) at low coverage on the pyramidal configuration and (f) at high coverage. Relative energies differences / magnetic moments are reported. Energy in eV, magnetic moments in Bohr magneton units.

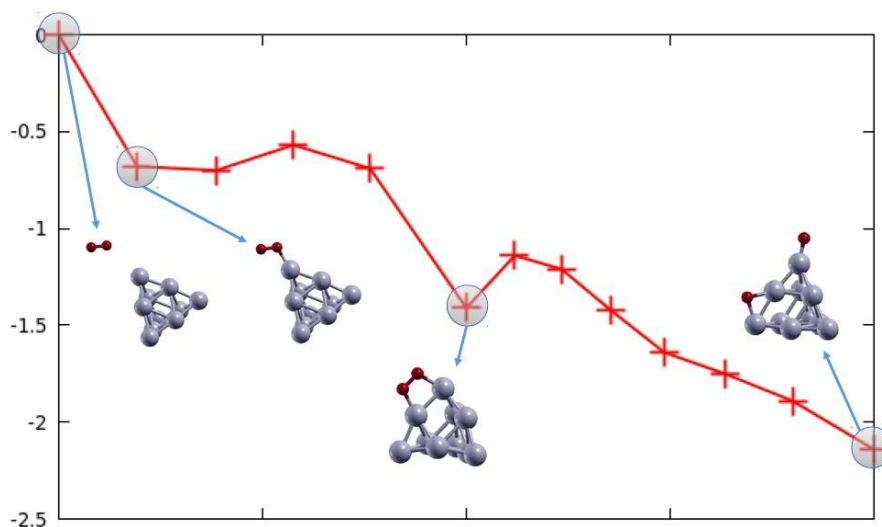


Figure S10. Breaking of O₂ on Pt₁₀ starting from O₂ in the gas phase and then adsorbed on a bridge site. Each red cross represents one NEB image. The energy barrier for O-O bond breaking is ≈ 0.3 eV.

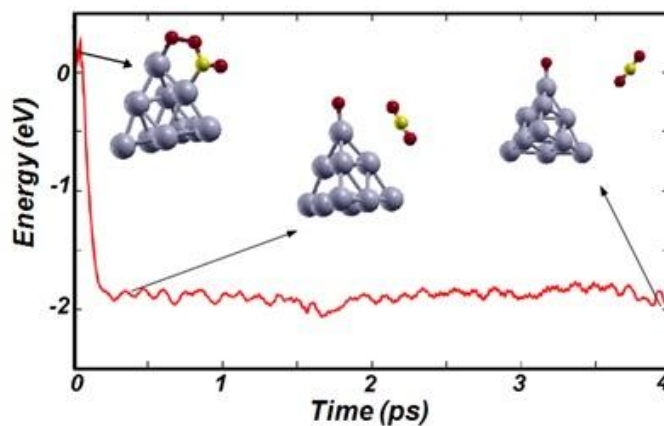


Figure S11. Plot of the energy as a function of time during a 4-psec Molecular Dynamics simulation at 300 K starting from a OOCO intermediate adsorbed on gas-phase Pt₁₀. Energies are in eV. Pt atoms are depicted in gray, oxygen in red and carbon in yellow. It can be noted that CO₂ simply detaches from the clusters into the gas phase without any hint of carbonate formation.

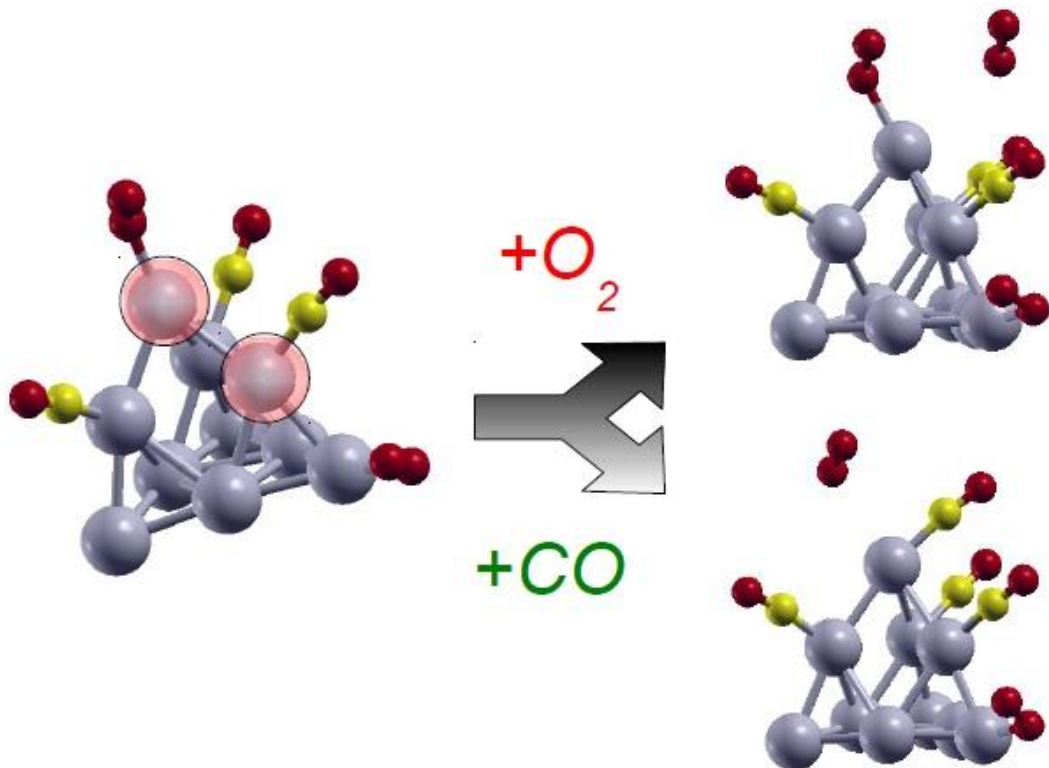


Figure S12. Results of local minimizations after adding one additional CO or O₂ molecule on the highlighted sites of the Pt₁₀(O₂)₂(CO)₃ cluster, showing desorption of CO or O₂ molecules initially positioned next to the cluster sites highlighted by circles (the species relax away into the gas phase) and thus proving that the cluster is locally saturated.

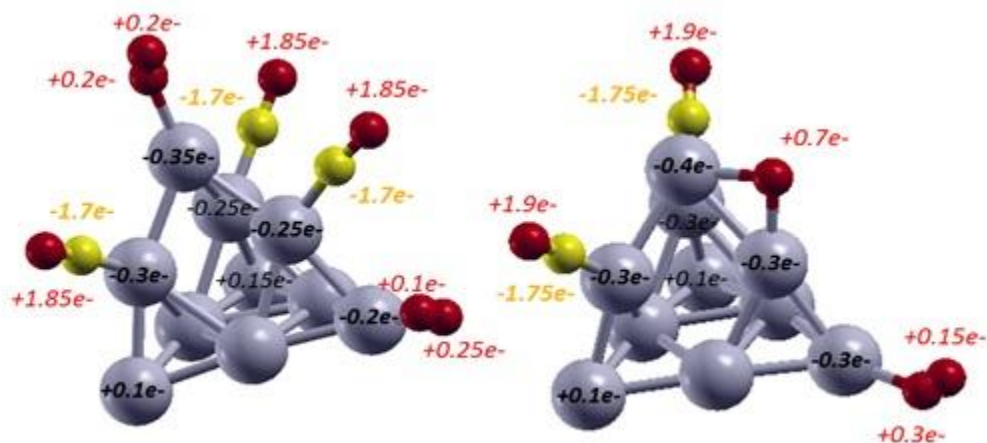


Figure S13. Bader charge analysis of two selected configurations: (left) Pt₁₀(O₂)₂(CO)₃ and (right) Pt₁₀O₂(CO)₂(O)₂ (note that in the right configuration one of the single O atoms is hidden by Pt), contrasting undissociated and dissociated O₂. A strong charge transfer from Pt₁₀ to O₂ (and to a lesser extent CO) which further increases when the oxygen molecule dissociates is clearly apparent from this figure.

References

1. Lee, S.; Molina, Luis M.; López, María J.; Alonso, Julio A.; Hammer, B.; Lee, B.; Seifert, S.; Winans, Randall E.; Elam, Jeffrey W.; Pellin, Michael J.; Vajda, S., Selective Propene Epoxidation on Immobilized Au₆-10 Clusters: The Effect of Hydrogen and Water on Activity and Selectivity. *Angew. Chem.* **2009**, *121*, 1495-1499.
2. Lei, Y.; Mehmood, F.; Lee, S.; Greeley, J.; Lee, B.; Seifert, S.; Winans, R. E.; Elam, J. W.; Meyer, R. J.; Redfern, P. C.; *et al.*, Increased Silver Activity for Direct Propylene Epoxidation via Subnanometer Size Effects. *Science* **2010**, *328*, 224-228.
3. Vajda, S.; Pellin, M. J.; Greeley, J. P.; Marshall, C. L.; Curtiss, L. A.; Ballentine, G. A.; Elam, J. W.; Catillon-Mucherie, S.; Redfern, P. C.; Mehmood, F.; Zapol, P., Subnanometre Platinum Clusters as Highly Active and Selective Catalysts for the Oxidative Dehydrogenation of Propane. *Nat. Mater.* **2009**, *8*, 213-216.
4. Deng, W.; Lee, S.; Libera, J. A.; Elam, J. W.; Vajda, S.; Marshall, C. L., Cleavage of the C-O-C Bond on Size-Selected Subnanometer Cobalt Catalysts and on ALD-Cobalt Coated Nanoporous Membranes. *Appl. Catal., A* **2011**, *393*, 29-35.
5. Vajda, S.; Winans, R. E.; Elam, J. W.; Lee, B.; Pellin, M. J.; Seifert, S.; Tikhonov, G. Y.; Tomczyk, N. A., Supported Gold Clusters and Cluster-Based Nanomaterials: Characterization, Stability and Growth Studies by *in situ* GISAXS under Vacuum Conditions and in the Presence of Hydrogen. *Top. Catal.* **2006**, *39*, 161-166.
6. Ferguson, G. A.; Yin, C.; Kwon, G.; Tyo, E. C.; Lee, S.; Greeley, J. P.; Zapol, P.; Lee, B.; Seifert, S.; Winans, R. E.; Vajda, S.; Curtiss, L. A., Stable Subnanometer Cobalt Oxide Clusters on Ultrananocrystalline Diamond and Alumina Supports: Oxidation State and the Origin of Sintering Resistance. *J. Phys. Chem. C* **2012**, *116*, 24027-24034.
7. Zhang, L. P.; van Ek, J.; Diebold, U., Spatial Self-Organization of a Nanoscale Structure on the Pt(111) Surface. *Phys. Rev. B* **1999**, *59*, 5837-5846.
8. Lee, S.; Lee, B.; Seifert, S.; Vajda, S.; Winans, R. E., Simultaneous Measurement of X-ray Small Angle Scattering, Absorption, and Reactivity: A Continuous Flow Catalysis Reactor. *Nucl. Instrum. Methods Phys. Res., Sect. A* **2011**, *649*, 200-203.
9. Ravel, B.; Newville, M., ATHENA, ARTEMIS, HEPHAESTUS: data analysis for X-ray absorption spectroscopy using IFFFIT. *Journal of Synchrotron Radiation* **2005**, *12*, 537-541.
10. Watanabe, Y.; Isomura, N., A New Experimental Setup for High-Pressure Catalytic Activity Measurements on Surface Deposited Mass-Selected Pt Clusters., *J. Vac. Sci. Technol., A*, 2009; Vol. 27, pp 1153-1158.
11. Giannozzi, P.; Baroni, S.; Bonini, N.; Calandra, M.; Car, R.; Cavazzoni, C.; Ceresoli, D.; Chiarotti, G. L.; Cococcioni, M.; Dabo, *et al.*, QUANTUM ESPRESSO: A Modular and Open-Source Software Project for Quantum Simulations of Materials. *J. Phys.: Condens. Matter* **2009**, *21*, 395502.
12. Perdew, J. P.; Burke, K.; Ernzerhof, M., Generalized Gradient Approximation Made Simple. *Phys. Rev. Lett.* **1996**, *77*, 3865-3868.
13. Vanderbilt, D., Soft Self-Consistent Pseudopotentials in a Generalized Eigenvalue Formalism. *Phys. Rev. B* **1990**, *41*, 7892-7895.
14. Kresse, G.; Furthmüller, J., Efficient Iterative Schemes for *ab initio* Total-Energy Calculations Using a Plane-Wave Basis Set. *Phys. Rev. B* **1996**, *54*, 11169-11186.
15. Blöchl, P. E., Projector Augmented-Wave Method. *Phys. Rev. B* **1994**, *50*, 17953-17979.
16. Ott, A. W.; Klaus, J. W.; Johnson, J. M.; George, S. M., Al₂O₃ Thin Film Growth on Si(100) using Binary Reaction Sequence Chemistry. *Thin Solid Films* **1997**, *292*, 135-144.
17. Bengtsson, L., Dipole Correction for Surface Supercell Calculations. *Phys. Rev. B* **1999**, *59* (19), 12301-12304.
18. Li, Z.; Scheraga, H. A., Monte Carlo-minimization approach to the multiple-minima problem in protein folding. *Proc. Natl. Acad. Sci. U. S. A.* **1987**, *84*, 6611-6615.
19. Aprà, E.; Ferrando, R.; Fortunelli, A., Density-Functional Global Optimization of Gold Nanoclusters. *Phys. Rev. B* **2006**, *73* (20), 205414.
20. Barcaro, G.; Aprà, E.; Fortunelli, A., Structure of Ag Clusters Grown on F_s-Defect Sites of an MgO(1 0 0) Surface. *Chem. Eur. J.* **2007**, *13*, 6408-6418.
21. Henkelman, G.; Uberuaga, B. P.; Jónsson, H., A Climbing Image Nudged Elastic Band Method for Finding Saddle Points and Minimum Energy Paths. *J. Chem. Phys.* **2000**, *113*, 9901-9904.

22. van Loenen, E. J.; Dijkkamp, D.; Hoeven, A. J.; Lenssinck, J. M.; Dieleman, J., Evidence for Tip Imaging in Scanning Tunneling Microscopy. *Appl. Phys. Lett.* **1990**, *56*, 1755-1757.
23. Højrup Hansen, K.; Worren, T.; Lægsgaard, E.; Besenbacher, F.; Stensgaard, I., Bias Dependent Apparent Height of an Al₂O₃ Thin Film on NiAl(110), and of supported Pd clusters. *Surf Sci* **2001**, *475* (1–3), 96-102.
24. Beniya, A.; Isomura, N.; Hirata, H.; Watanabe, Y., Morphology and Chemical States of Size-Selected Pt_n Clusters on an Aluminium Oxide film on NiAl(110). *Phys. Chem. Chem. Phys.* **2014**, *16*, 26485-26492.
25. Yoshitake, M.; Lay, T.; Song, W., Well-Ordered Ultra-Thin Al₂O₃ Film Formation on NiAl(110) by High-Temperature Oxidation. *Surf Sci* **2004**, *564*, 211-217.